Journal of Energy Storage 77 (2024) 109964

Contents lists available at ScienceDirect

Journal of Energy Storage

journal homepage: www.elsevier.com/locate/est

Research papers

Numerical investigation on the thermal management of Li-ion batteries for electric vehicles considering the cooling media with phase change for the auxiliary use

Ahmet Mavi [a], Oguz Arslan [b,*]

[a] Vocational School, Bilecik Şeyh Edebali University, Bilecik, Turkey
[b] Department of Mechanical Engineering, Faculty of Engineering, Bilecik Şeyh Edebali University, Bilecik, Turkey

ARTICLE INFO

Keywords:
Li-ion battery
Numerical analysis
Thermal management
Two-phase flow

ABSTRACT

This study investigates the thermal management of a battery module of an electric vehicle for the recovery of waste heat. In the evaluation of this waste heat, a two-phase flow system is used to provide a more effective heat transfer. The battery system was formed of 6 serial connected prismatic Lithium-Ion cells. It was aimed to design a 134.55 kW electric vehicle battery system. For this aim, 360 battery modules were used. The maximum amount of waste heat obtained from these modules was recorded as 6.192 kW. Since it is aimed to use this waste heat in the auxiliary cycles such as air conditioning and extra electricity production, R600a was used as the cooling media. A parametric study was conducted for different discharging rates (C) and depths of discharging (DoD) through computational fluid dynamics (CFD) for performing the thermal analysis of the battery module. The heat transfer coefficient was determined ranging between 1.10 and 5.49 $kWm^{-2}K^{-1}$. The cooled module temperature was recorded between 290.93 K and 317.31 K, whereas it was recorded as 332.57 K for the non-cooled system. For secondary purposes, the refrigerant mass rate ranging between 0.2760 kgs^{-1} and 0.6559 kgs^{-1} was obtained in a temperature range of 283 K and 313 K.

1. Introduction

Electric vehicles provide many benefits, including environmental sustainability, energy independence, and economic advantages. Therefore, the prevalence of electric cars will play an essential role in the transportation sector in the future. The automotive industry faces undesirable situations such as energy deficiencies and air pollution [1]. Electric and hybrid electric vehicles have greater energy capacity than fossil fuel and are environmentally friendly [2,3]. The lithium-ion batteries (Li-ion batteries) employed in electric vehicles are preferred over fossil fuel vehicles since they have many gains, including specific energy, fast charging, being environmentally friendly, and having a lower weight [4,5]. The use of electric vehicles is becoming widespread to minimize the damage caused by emissions from vehicles to human health and the environment. If the energy needs of electric vehicle charging stations are met by renewable energy, the use of electric vehicles will become more widespread. Due to the limited availability of fossil fuels, which are widely used in the transportation sector, their high dependence on foreign sources, and their harmful emissions, the use of energy obtained from renewable sources in electric vehicles makes it even more attractive today [6,7]. Lithium-ion batteries have overheating problems during charging and discharging, negatively impacting battery life and performance. In addition, as the battery temperature rises, the chemical reactions occurring inside the battery accelerate, which shortens the life of the battery. Therefore, the cooling process of lithium-ion batteries is essential to extend the battery life and improve performance [8]. Preventing high temperatures in battery units, minimizing temperature differences, and keeping the units within the desired operating temperature range prevent negative situations that may occur in the battery [9]. If the cooling efficiency of the batteries is insufficient, the discharge performance of the batteries, shortening of their life, and thermal leaks may occur. It causes undesirable conditions such as thermal runaway formation in the battery, exothermic reactions, ignition, and battery explosion. To ensure the long-term use of Li-ion batteries and the safety of the battery set, Li-ion battery cells should be designed in the best geometric shapes, and battery thermal management should be performed under appropriate cooling conditions [10]. The importance of cooling Li-ion battery units was increased to reduce the

* Corresponding author.
E-mail address: oguz.arslan@bilecik.edu.tr (O. Arslan).

https://doi.org/10.1016/j.est.2023.109964
Received 27 July 2023; Received in revised form 15 November 2023; Accepted 2 December 2023
Available online 15 December 2023

high temperatures and prevent heterogeneous temperature distribution [11,12]. Li-ion batteries should be controlled at extremely high temperatures in addition to the harmful factors in the normal working process. It is seen that the formation of thermal runaways occurs at temperatures of 80 °C and above in the battery [13]. For this reason, the importance of the battery thermal management system (BTMS) is to keep the battery in the desired operating temperature conditions. The excellent design of thermal systems is essential in extending battery life, obtaining maximum power from the battery, and safe battery operation. [14–16]. For using the batteries effectively, the ideal temperature of the batteries specified in the battery user manual should be 20 °C–40 °C [17]. One of the methods for cooling lithium-ion batteries is applying coolant directly to the batteries. In this way, it is possible to recover some part of the generated heat by cooling the batteries, which can increase energy efficiency [18].

The rate at which the battery can be charged or discharged is called the C-rate. Another explanation of the C-rate is the magnitude of the current to be applied during the one-hour charge/discharge period. Except for the operating environment and the C ratio, the heat transfer coefficient (h) directly impacts the battery's thermal properties [19,20]. Thermochemical and electrical properties of the lithium-ion battery, 5 $Wm^{-2}K^{-1}$, 10 $Wm^{-2}K^{-1}$, and 25 $Wm^{-2}K^{-1}$ at various convective heat transfer coefficients, and it was investigated at ambient temperatures of 0 °C to 25 °C, at different rates of 0.5C, 1C and 1.5C [21]. Yetik and Karakoç [22] suggested a thermal system evaluation for $LiMn_2O_4$-graphite prismatic battery by evaluating natural and forced convection conditions at various discharge rates of 0.5C, 1.0C, 2.0C, and 2.5C. A tiny alteration in the heat transfer coefficient alters the battery temperature. For this reason, the convective heat transfer coefficient is vital for keeping the battery heat at the desired level and controlling it.

Many studies were conducted in the literature to develop thermal management systems for Li-ion batteries, including preventing sudden temperature increases in the battery, eliminating thermal runaways, and keeping temperatures under control [23]. The most used methods in batteries are air cooling [24], liquid cooling [25], cooling with phase change materials [26], heat pipes [27], and different thermal systems designed in conjunction with the methods mentioned above [28,29]. Air cooling systems are widely used because the cost is cheaper than other systems. Air cooling systems become insufficient when the battery capacity and the number of batteries are increased. Although liquid cooling systems are complex systems that negatively affect the vehicle's weight, they are widely used for cooling electric vehicle batteries [30–32]. Problems arise when phase change materials (PCMs) are used in vehicles. The cost of heat pipes is higher in comparison to other systems, and they are affected by gravity. PCMs and heat pipes are not preferred due to the negativities during the cooling process [33–36]. A hybrid cooling system was designed with 3 different cooling methods. The evaporation energy of water was used to increase the cooling efficiency of the battery module. It was concluded that using the hybrid cooling method reduces the pump power and required air flow rate for the cooling design. They stated that this situation will contribute to the energy requirement of the electric vehicle to some extent [37]. To increase the performance of electric vehicles, analysis of different cooling channels was carried out with ANSYS. In a design where water is used as the coolant, a rectangular design yielded good results. It was also been observed that curved channels provide a more effective performance than open channels [38].

The dual-phase refrigerant model can be preferred in thermal management systems as an alternative to current cooling media. The heat generated in the battery can be removed from the system much faster than traditional methods depending on the higher heat convection value. The dual-phase fluid cooling method has been investigated for many devices [39]. The samples include the fuel cells with polymer electrolyte membranes (PEMFC) in which heat is generated by the thermochemical reaction as in Li-Ion batteries [40,41]. However, an additional cooling unit is needed for these kinds of systems. For an electric vehicle (EV), the cooling units used in existing air conditioning (AC) systems can be made compatible with two-phase refrigerants by making minor changes [42–44]. Gao et al. [45] perform a thermal analysis of the battery module. R410a was chosen as the refrigerant directly applied to the module. Regarding their work, they proposed a new safety thermal system integrated with the cooling system. Al-Zareer et al. [46,47] performed a thermal analysis of a battery pack cooled with R134a. They placed the batteries inside the battery pack filled with refrigerant. In this method, a cooling design is carried out for each battery. So, they stated that the cooling process occupies a considerable area. Park et al. [48] studied the thermal management of the battery using mini-channel heat sinks. They used R134a as the heat transfer media. According to the results of the cooling analysis carried out with the dual-phase fluid, the cooling process showed an excellent performance depending on the independence of the ambient temperature. In batteries, cooling system designs with dual-phase refrigerant provide a successful solution to ensure the ideal operating temperature range of the battery. The system can be directly integrated into the vehicle air conditioner [49]. The two-phase immersion cooling method was experimentally evaluated in 18,650-type Li-ion battery cells under different operating conditions. Different cooling systems, including natural cooling, forced convection, mineral oil, and SF33 dual-phase fluid, were compared. Due to its high heat transfer efficiency, two-phase liquid cooling has shown that it can be effectively used in the thermal management of lithium-ion batteries. SF33 showed that dual-phase cooling has a superior cooling performance compared to other systems [50]. A study on a two-phase liquid immersion cooling system used in data centers evaluated the reliability and energy efficiency of a newly designed two-phase cooling system for data centers. It is seen that the two-phase cooling system examined in this study gives better results than other systems [51]. In the experimental study, dual-phase fluid was used to cool the battery pack. It was stated that the cooling process of the cells was examined by the direct contact method by taking advantage of the liquid-vapor phase change feature of the fluid. In the research, the effect of refrigerant height and different discharge rates on maximum temperature was examined. Increasing the immersion height further reduces the maximum battery temperature, especially when the discharge rate is high [52]. The cylindrical LiFePO4 lithium-ion battery was operated at different discharge rates between 4C and 10C. It has been observed that the immersion cooling method provides effective heat transfer from the battery surface when the fluid transitions to a dual-phase state. Under the same conditions, this method appears to provide superior performance compared to single-phase liquid immersion cooling [53]. Recently, it has been argued that the use of dual-phase fluids in the thermal analysis of batteries will gradually increase. They stated that the battery temperature is more homogeneous thanks to the phase change of the dual-phase fluid used, but when compared to this cooling system with traditional methods, these fluids must have some properties due to the flammable properties of the dual-phase fluids. At the same time, dual-phase fluids are lightweight, making them more attractive to use for electric vehicles [54].

Thanks to the high latent heat of evaporation of the fluid, the heat released during the operation of the battery module can be transferred more effectively. In addition, the temperature distribution obtained from the battery module would be very smooth since the temperature of the refrigerant is almost equal during the cooling process. In this study, a $LiMn_2O_4$ lithium-ion prismatic battery with 14.6 Ah was performed for an electric vehicle. The battery unit was designed in the form of 6 serial connected batteries. The unit was evaluated at different C-rates. In the thermal management system, the battery unit was considered an evaporator of the vehicle's auxiliary subsystem. The refrigerant R600a was chosen as the cooling media to remove the waste heat generated by the battery unit since it was aimed to evaluate the working fluid for extra aims, such as air-conditioning and electricity generation in the auxiliary cycles. In this regard, different inlet temperatures and mass ratios were evaluated to provide suitable working environments for the batteries.

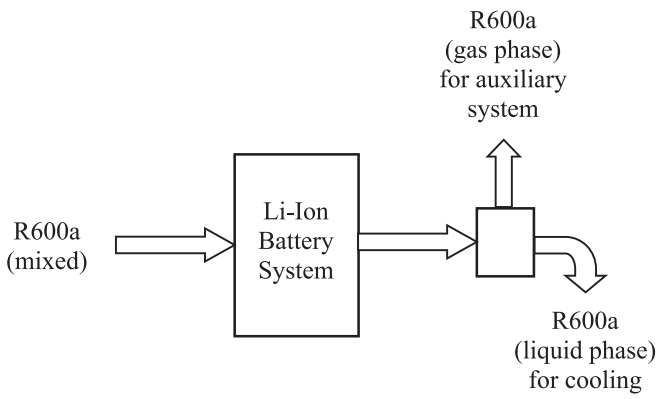

Fig. 1. Schematic of the dual-phase thermal management system.

The heat transfer coefficients were determined parametrically considering the phase change. In this regard, computational fluid dynamics (CFD) analyses for the thermal behavior of the lithium-ion battery were performed.

2. Material and method

This study aims to obtain thermal management of a Li-ion battery system through two-phase heat transfer depending on the higher heat transfer coefficients. Thus, the removed heat from the battery would be used for the second aim as well as to obtain a homogenous surface temperature for an efficient operation. The schematic of the thermal management system is given in Fig. 1.

According to Fig. 1, R600a was chosen as the cooling media due to its common use in refrigeration systems and environmental properties, such as global warming and ozone depletion potential. The generated heat in the Li-ion cell is removed during the boiling process of R600a. Later, the gas and liquid phases are separated. The gas phase is directed to an auxiliary system to be used for the second purpose, such as a mini-ORC, thermoelectric generator, or refrigeration cycle. The battery unit is modeled in consideration of the prismatic Li-ion battery cell. The battery unit includes six prismatic batteries in a series connection. A prismatic Li-ion battery with a capacity of 14.6 Ah and a size of 192 × 145 × 5.4 mm was employed in the analyses. The battery contains a $LiMn_2O_4$ cathode and graphite-based anode. Fig. 2 shows the battery unit used for analysis. Battery information is shown in Table 1.

2.1. CFD analysis

The Newman-Tiedemann-Gu-Kim (NTGK) model is a mathematical model developed to analyze the electro-thermal process of Li-ion batteries. The NTGK model examines the internal structure of the battery to calculate electro-thermal interactions in detail. This model includes factors such as conductivity between electrodes, diffusion between electrodes and electrolyte, electrochemical reactions on electrode surfaces, and internal resistance of the battery. It contains thermal equations to calculate the heat generated and temperature distribution inside the battery, depending on these factors. Temperature and thermal analyses of the battery unit were examined with the NTGK model in the ANSYS Fluent program, taking into account the initial temperatures, different refrigerant inlet temperatures, and different C ratios. [55,56]. Polarization values and equations used in the model are given by Ref. [56–59]:

$$\frac{\partial \rho C_p T}{\partial t} = \sigma_+ |\nabla \varphi_+|^2 + \sigma_- |\nabla \varphi_-|^2 + Q_g \quad (1)$$

$$\nabla.(\sigma_+ \nabla \varphi_+) = -(J_{ECh} - J_{short}) \quad (2)$$

Table 1
Specifications of Li-ion battery.

Specifications	Value
Battery capacity	14.6 Ah
Maximum voltage	4.2 V
Minimum voltage	3.0 V
Cathode material	$LiMn_2O_4$
Anode material	Graphite
Electrolyte	Polymer-based
Dimensions (mm)	192 × 145 × 5.4
Cooling plate (cover)	Aluminum; 192 × 145 × 3

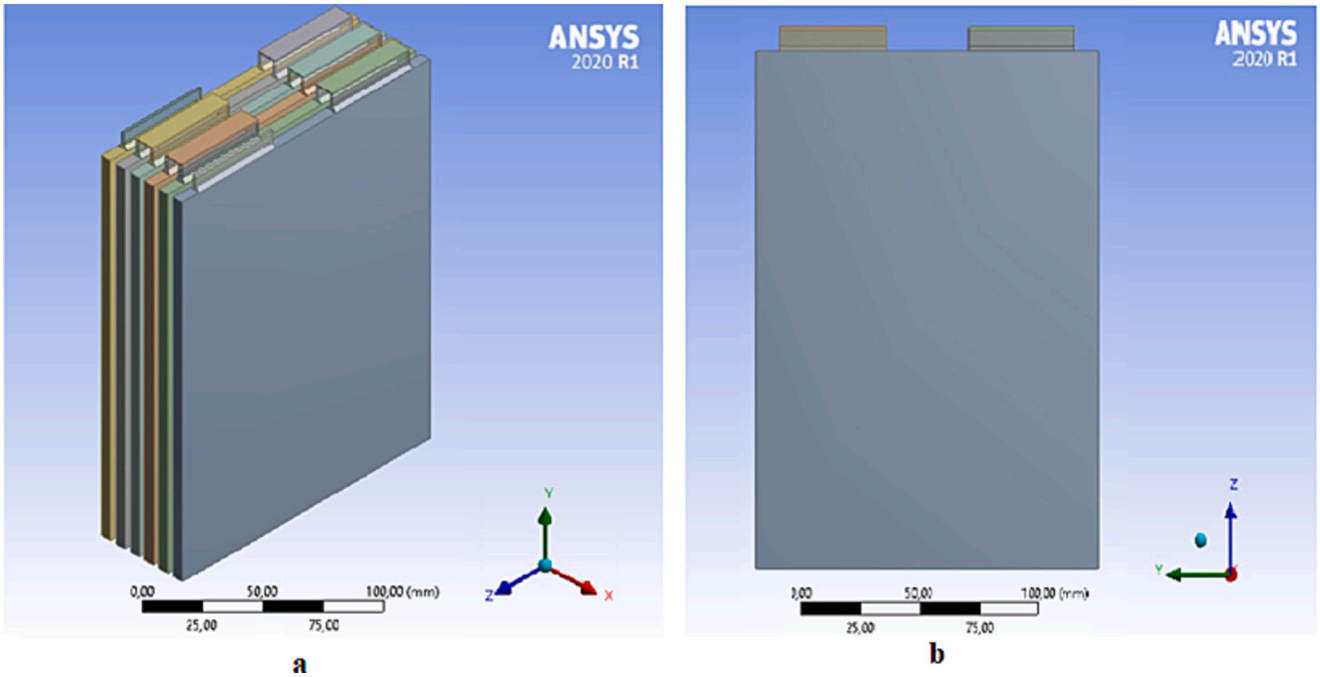

Fig. 2. The 3D appearance of the battery unit (a) and in the XY plane (b).

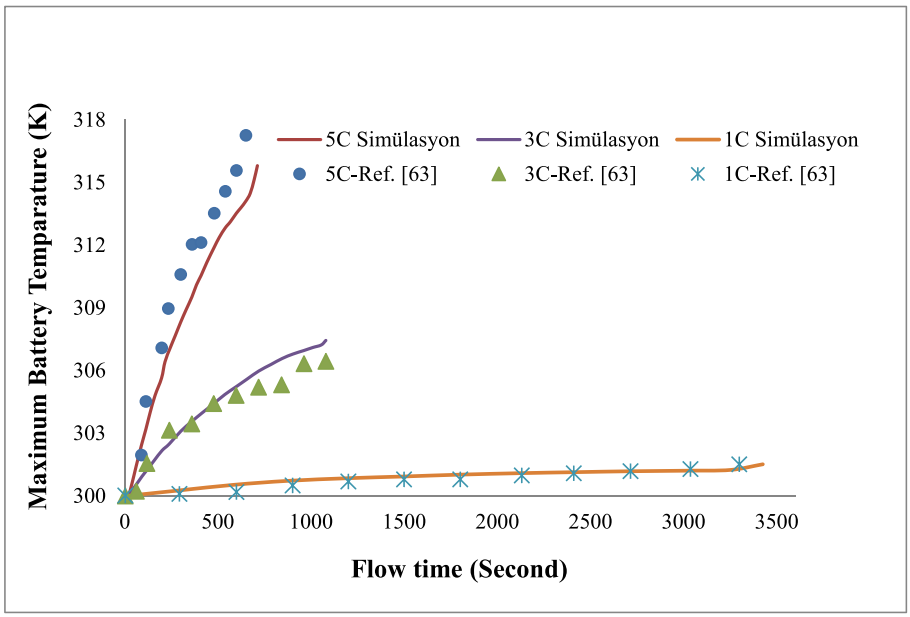

Fig. 3. Validation of simulation results.

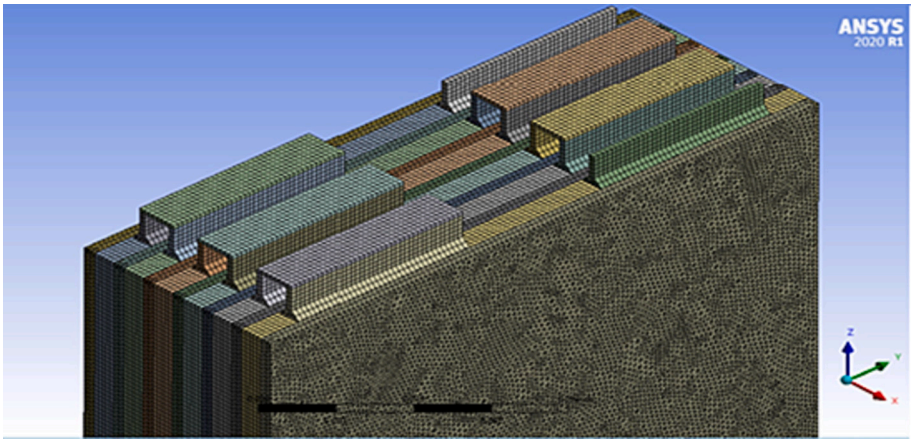

Fig. 4. Mesh structure.

$$\nabla.(\sigma_{-}\nabla\varphi_{-}) = (J_{ECh} - J_{short}) \tag{3}$$

$$J_{ECh} = \alpha Y[U - (\varphi_{+} - \varphi_{-})] \tag{4}$$

The terms σ_+ and σ_- in the equation represent the positive and negative electrical conductivity of electrons, and the terms, φ_+ and φ_- represent the phase potentials of positive and negative electrodes. Q_g gives the amount of heat produced in the cell. J_{ECh} is the volumetric current delivery rate, and J_{short} is the current conductivity rate. Y and U represent the open-circuit potential voltages of the battery as variables that vary with the battery's discharge level [60,61]. U and Y values were obtained using the experimental studies [56,59,62]:

$$U = a_0 + a_1(\text{DoD}) + a_2(\text{DoD})^2 + a_3(\text{DoD})^3 \tag{5}$$

$$Y = a_4 + a_5(\text{DoD}) + a_6(\text{DoD})^2 \tag{6}$$

Here a_0-a_6 are the coefficients obtained due to the polynomial curve [63]. The DoD value is given by Ref. [56]:

$$\text{DoD} = \frac{V_b}{3600\, Q_{Ah}}\left(\int_0^t j dt\right) \tag{7}$$

where V_b is the battery voltage, J is the current density, t is the flow time during the discharge process, and Q_{Ah} is the capacity (Ahm^{-2}) of the electrodes. The heat transfer is managed by the conductive equality with the heat source component [56]:

$$\frac{\partial \rho C_p T}{\partial t} - \nabla.(k\nabla T) = \dot{q} \tag{8}$$

where k gives the thermal conductivity and Cp the thermal capacity of the battery. The heat transfer from the battery surface to the external environment is given by ref. [56]:

$$q = h(T_s - T_b) \tag{9}$$

where q is the heat flow, and h is the heat transfer coefficient. T_s and T_b are the surface temperatures and the ambient temperature. The controlling equations of continuity and momentum are given as follows:

$$\frac{\partial \rho}{\theta t} + \nabla.(\rho \vec{v}) = 0 \tag{10}$$

$$\frac{\partial \vec{u}}{\theta t} + (\vec{v}\nabla)\vec{v} = -\frac{\nabla_p}{\rho} + \frac{\mu}{\rho}.\nabla^2\vec{v} = 0 \tag{11}$$

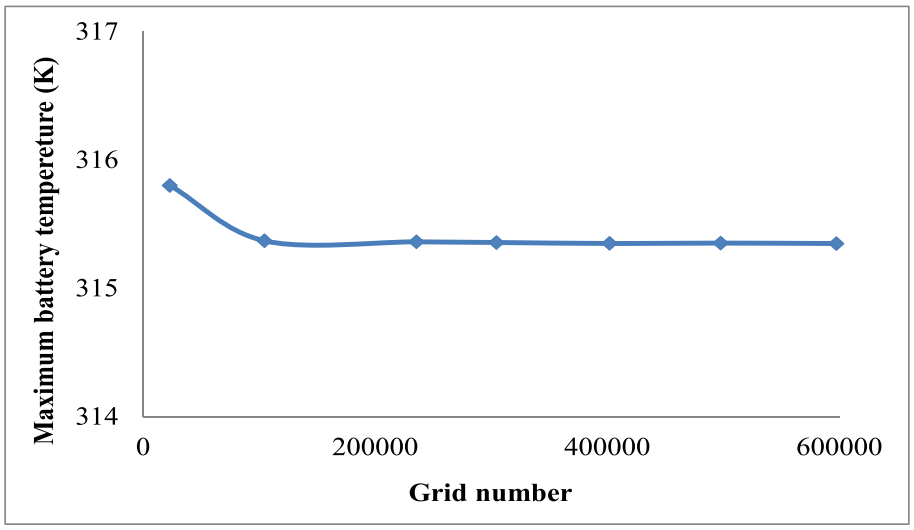

Fig. 5. Grid independence of mesh structure.

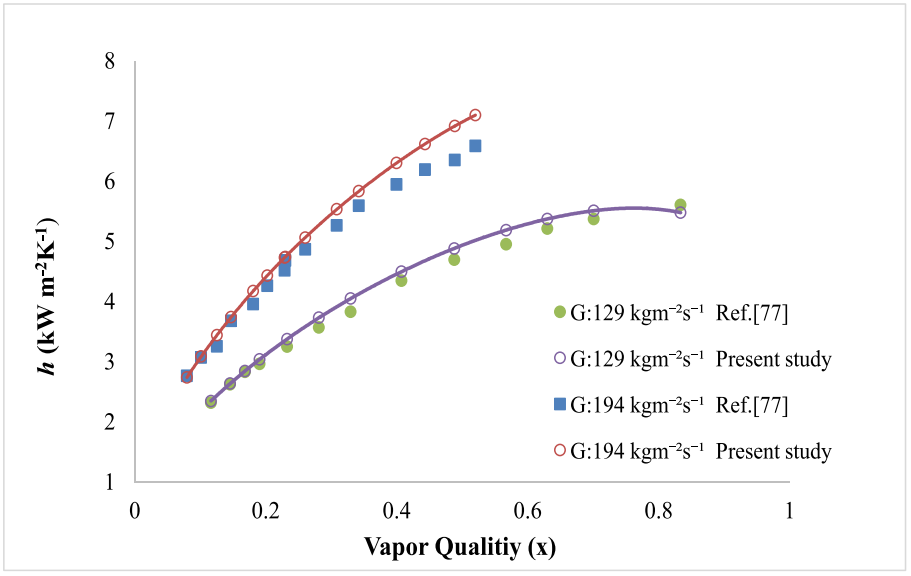

Fig. 6. Validation of heat transfer model [77].

Simulation results obtained by CFD analysis were compared with those of Ref. [63] performed for the validation. The alterations in battery temperatures with flow time for analysis results (current study) and experimental results are given in Fig. 3.

According to Fig. 3, the correlation coefficients (R^2) were found to be 0.963, 0.971 and 0.987. Mean average percentage error (MAPE) values were determined to be 0.3580 %, 0.1635 % and 0.5538 %. The obtained results are highly compatible with the experimental findings. Thus, it has been proven that the battery model can be used with high accuracy. The meshing was conducted by the hybrid mesh structure. The overall mesh structure of the $LiMn_2O_4$ battery unit is presented in Fig. 4.

The NTGK model was used for different mesh number conditions at a 5C rate. In the analysis, the ambient temperature was accepted as 300 K. The thermal variation of the maximum cell temperature based on the increase in the number of cages is given in Fig. 5.

According to Fig. 5, temperature alterations are given depending on the mesh number. Accordingly, it was observed that the battery temperature lowered from 315.3618 K to 315.3567 K depending on the increase in the number of elements from 235,638 to 304,535. According to this result, the alteration in terms of the maximum battery temperature was 0.051 K. The mesh independence test was sufficient to perform a 304,535 element count analysis.

2.2. Heat generation

The heat rates generated by the operation of the battery module are required to perform the thermal analysis of the battery module effectively. The Bernardi formula is generally used to determine the heat generation obtained from lithium-ion batteries [64]. Heat generation occurs due to electrochemical reactions occurring in the battery cell. The heat generated in the battery generally consists of reversible, irreversible side reactions and mixing heat. Irreversibility generally increases as the amount of current applied to the battery increases. During the discharge of the battery, the joule heat generated due to electrochemical reactions is encountered as heat generated due to side reactions and mixing heat. The heat of mixing and side reactions are mostly negligible [65–69]. The heat production equation in the cell, which is widely used by Bernardi et al., is expressed as follows [70].

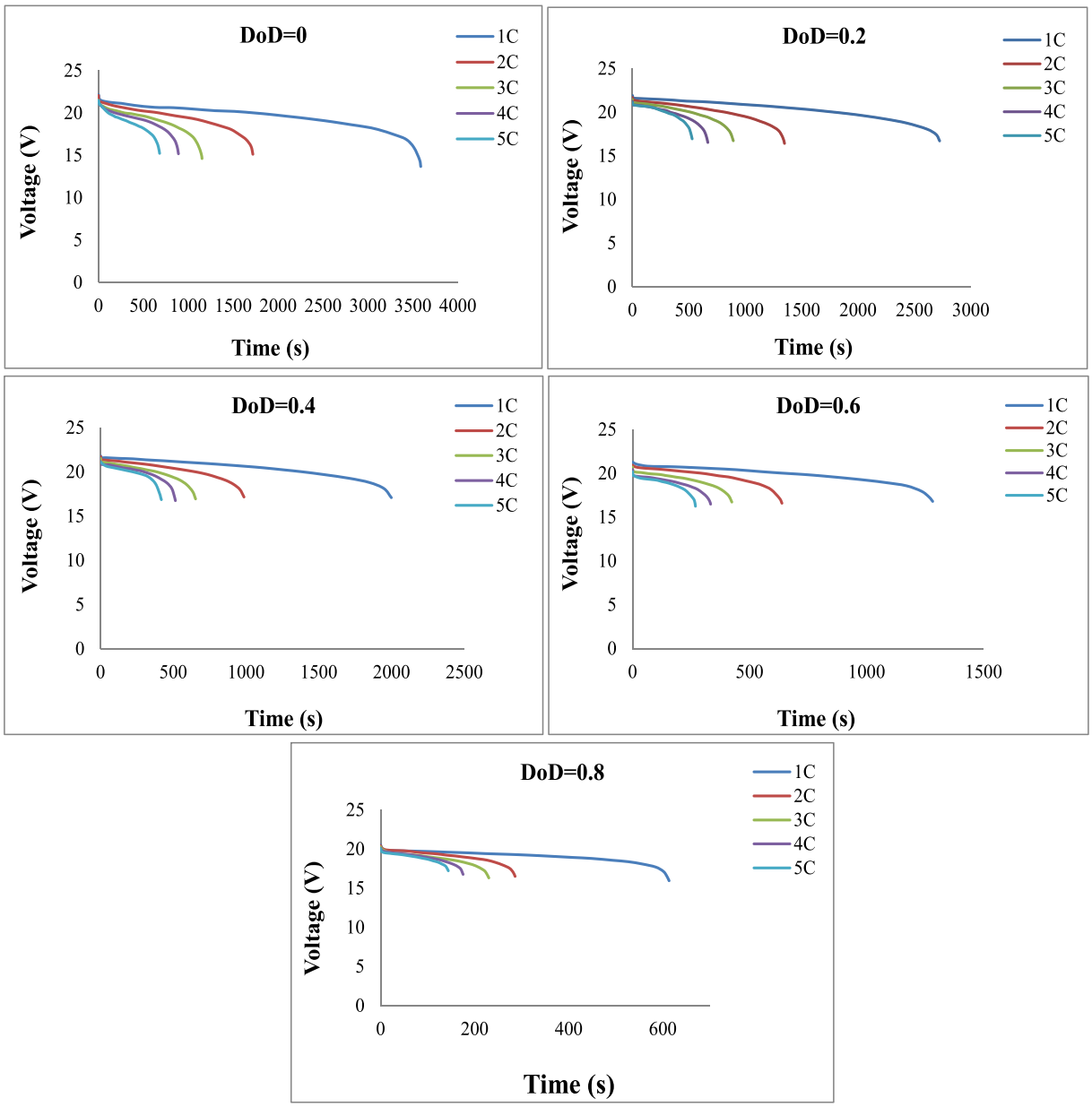

Fig. 7. Voltage variations for different DoD levels.

$$q = I^2R(I, SOC) - IT\frac{\partial E(SOC)}{\partial T} \tag{13}$$

$$q_j = I^2R(I, SOC) = I(E(SOC) - U(I, t)) \tag{14}$$

where q is the heat generation rate, and I is the discharge current applied to the battery. R is resistance, T is the battery temperature, E is the open circuit Voltage, U is the terminal voltage, q_J is the Joule heat, SOC is the state of charge, and $IT\frac{\partial E}{\partial T}$ is heat that occurs by reversible electro-chemical reactions. According to Eq. (13), the heat generation rate of the battery varies depending on the ambient temperature, discharge rate, and direct current (DC) resistance. The irreversible Joule heat depends on the battery's DC resistance. DC resistance essentially consists of ohmic and polarization resistance [71]. Irreversible Joule heat can be preferred as a heat source compared to non-reversible [72].

The heat dissipation in the battery cell can be considered as the mass point, with constant heat generation and a constant internal temperature at any time. For this reason, using the lumped parameter method in solving the heat transfer equations of the battery will help solve the problems more straightforwardly than the complex structure [68]. The thermodynamic properties, such as temperature and heat generation at a particular time (t), are estimated by minimizing the time intervals during battery discharge.

2.3. Heat transfer modeling

The convective heat transfer coefficients for the two-phase flow were considered in the model. In controlling the temperature of the battery unit, it was assumed that the surface of the cooling plate was made of aluminum. The unit was handled as an evaporator to evaluate the waste of the heat transferred from the battery surface. In this aim, a heat transfer model based on a phase change process was proposed. R600a is selected as cooling media, which can later be evaluated in the auxiliary systems such as organic Rankine cycle (ORC), thermoelectric unit, or cooling cycle [73–75]. The heat transfer coefficient (h) for the two-phase (boiling) fluid is given as the sum of the bubble boiling (h_k) and the forced convection coefficients (h_z) [76]:

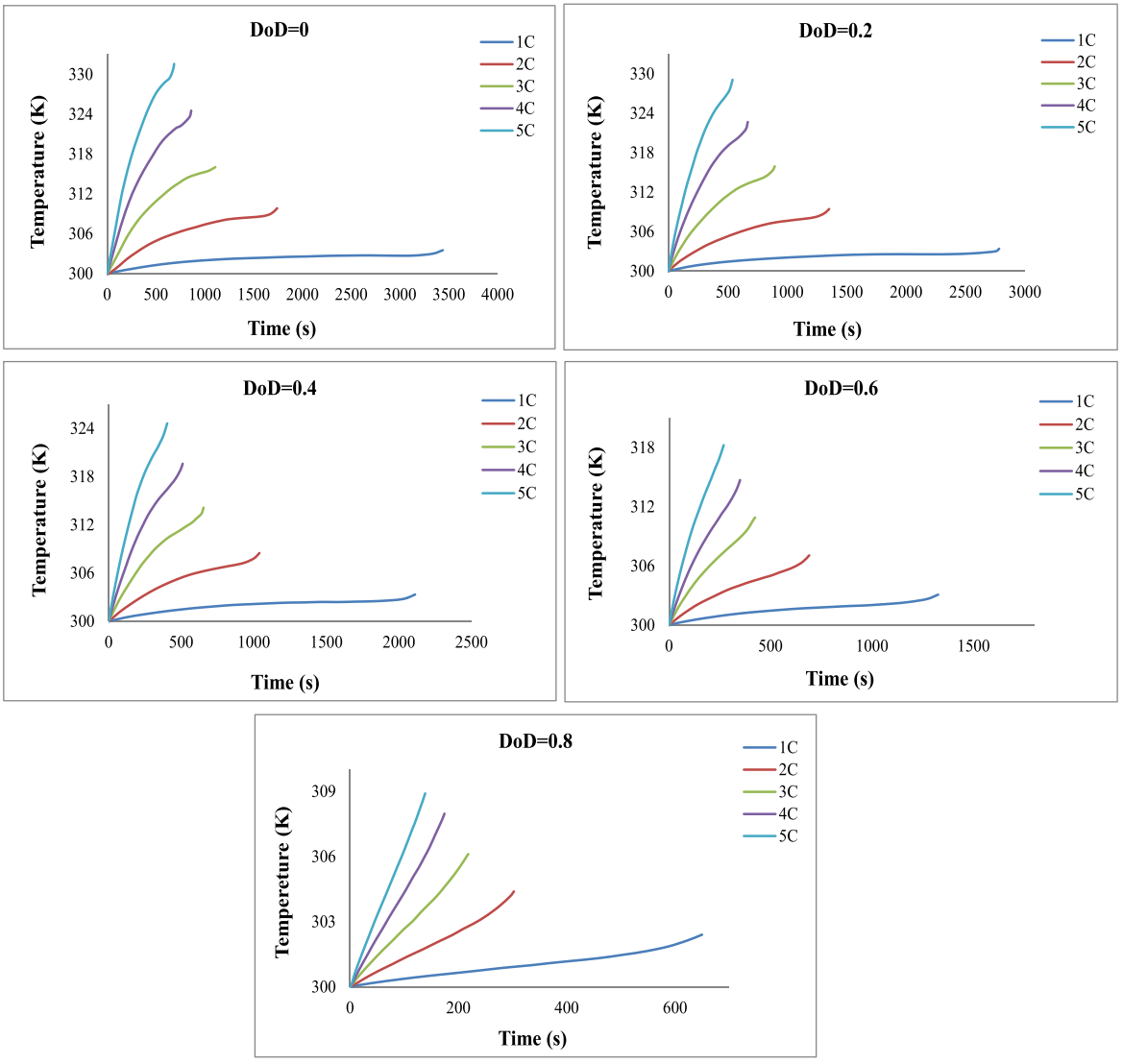

Fig. 8. Temperature variation for the non-cooled case.

$$h = h_k + h_z \tag{15}$$

where

$$h_k = 0,023\left(\frac{G.(1-x).D}{\mu_f}\right)^{0,8} Pr_f^{0,4}\frac{\lambda_f}{D}.F \tag{16}$$

$$h_z = 0,00122\left(\frac{k_f^{0,79} C_{pf}^{0,45} \rho_f^{0,49}}{\sigma^{0,5}\mu_f^{0,29} h_{fg}^{0,24} \rho_g^{0,24}}\right)\Delta T_d^{0,24}\Delta P_d^{0,75} S \tag{17}$$

Here, ΔT_d is assigned as the difference between the battery surface temperature (T_w) and the saturation temperature of the fluid (T_s), where ΔP_d is the difference between the saturation pressure at T_w and the saturation pressure of the fluid at T_s. F, S, G, σ, x, μ, ρ, and k are defined as forced convection-boiling factor, effectiveness factor, mass velocity, surface tension, dryness factor, dynamic viscosity, density, and conductivity, respectively. The subscripts of f and g indicate the properties at saturated liquid and vapor points, respectively. In terms of the Martinelli parameter (X_{tt}), F is defined by [76]:

$$\begin{aligned} F &= 1.0 && \frac{1}{X_{tt}} \le 0.1 \\ F &= 0.235\left(\frac{1}{X_{tt}} + 0,213\right)^{0,736} && \frac{1}{X_{tt}} > 0.1 \end{aligned} \tag{18}$$

where

$$X_{tt} = \left(\frac{1-x}{x}\right)^{0,9}\left(\frac{\rho_g}{\rho_f}\right)^{0,5}\left(\frac{\mu_f}{\mu_g}\right)^{0,1} \tag{19}$$

In terms of Re number, S is given by [76]:

$$\begin{aligned} S &= \left(1 + 0,12Re^{1,14}\right)^{-1} && Re \le 32.5 \\ S &= \left(1 + 0,42Re^{0,78}\right)^{-1} && 32.5 < Re < 70 \\ S &= 0.1 && Re \ge 70 \end{aligned} \tag{20}$$

where Re is given in terms of F [76]:

$$Re = F^{1,25}\left(\frac{G.(1-x).D_h}{\mu_f}\right) \tag{21}$$

where D_h is defined as the hydraulic diameter considering a rectangular cross-section. The proposed model was validated with the literature

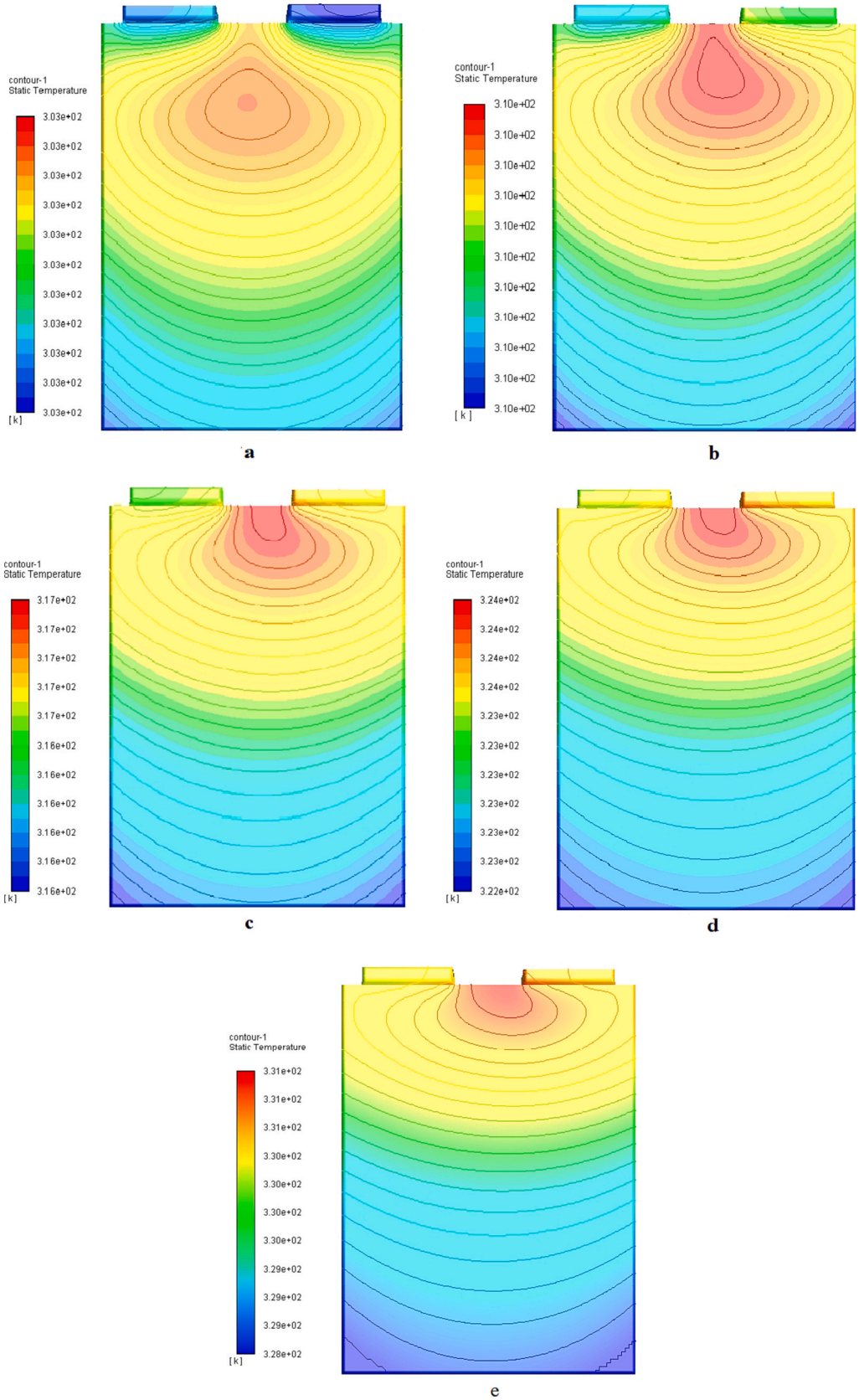

Fig. 9. The temperature variations of the battery surface for the non-cooled case; a) 1C, b) 2C, c) 3C, d) 4C, e) 5C.

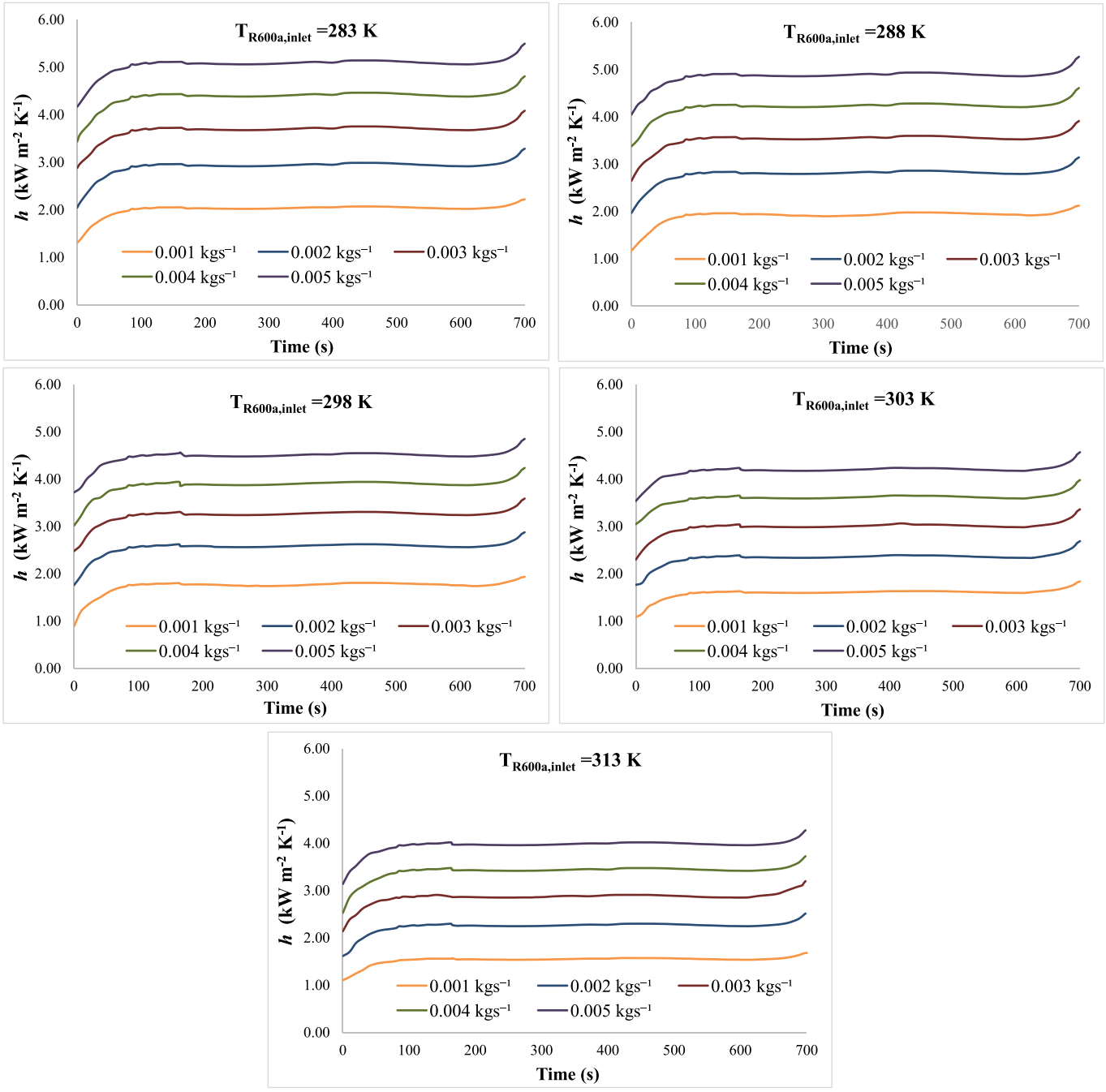

Fig. 10. Variation of heat transfer coefficients for different inlet temperatures at 5C.

data, and the results are given in Fig. 6.

According to Fig. 6, R^2 values were obtained as 0.9934 and 0.9926, whereas MAPE values were obtained as 4.4903 % and 2.5882 %. The results show that the simulated model is highly compatible.

3. Results

In this article, the NTGK model was applied considering different discharge conditions to provide numerical thermal data from a $LiMn_2O_4$ battery unit bearing a nominal capacity of 14.6 Ah and 25.2 V. CFD analysis was conducted at 27 °C ambient temperature neglecting the busbar effects via ANSYS battery tool. In CFD analysis, the boundary conditions were selected as temperature and velocity of the cooling fluid. According to this, the non-cooled case was investigated first. In this case, the natural convection conditions (h = 5 Wm^{-2} K^{-1}) were evaluated for a baseline. The voltage variation results are given in Fig. 7.

According to Fig. 7, it can be seen that the decreasing trends of battery voltage are similar at different DoD values. As the C ratio increases, the tendency of the battery voltage to decrease also increases. It is seen that the maximum operating times of the battery cell also change at different C ratios. Discharge times vary according to the magnitude of the current applied to the battery. The longest discharge time is at 1C, and the shortest discharge time is at 5C. The higher the DoD value, the lower the battery voltage. Also, higher C ratios mean faster drops in battery voltage. Towards the completion of the discharge, the battery voltage drops rapidly due to the depletion of lithium ions on the anode side. This rapid drop in voltage leads to an increase in irreversible heat caused by chemical reactions.

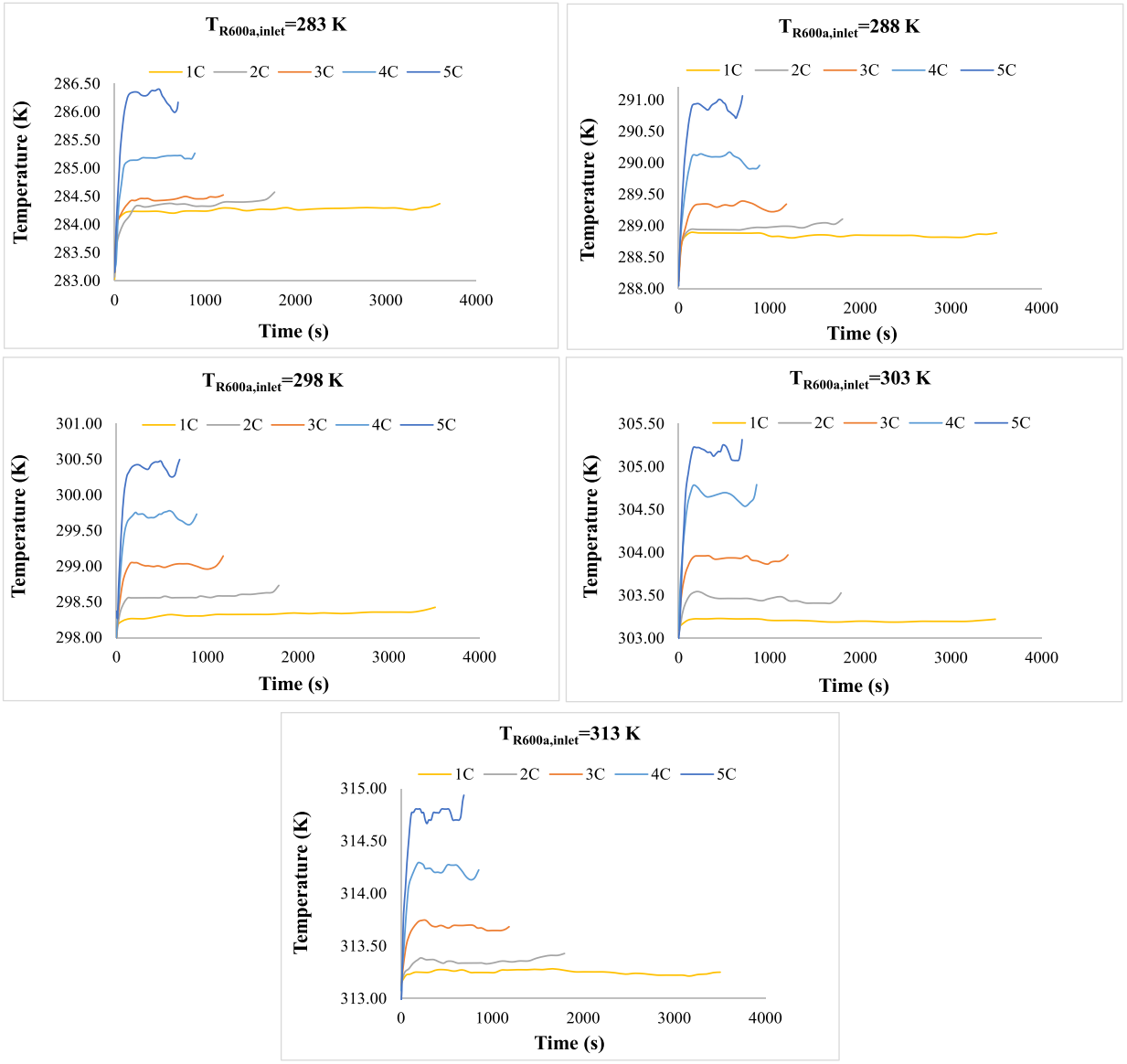

Fig. 11. Variation of battery surface temperature for the cooled case (m = 0.005 kg s^{-1}).

The irreversible Joule heat is expressed in proportion to the decrease in Voltage and discharge rate. Therefore, a significant amount of heat is generated in the battery during high-speed discharges. The amount of heat produced in the designed battery module varies depending on the different operating conditions of electric vehicle batteries. One module of the battery pack at 5C discharge rate has a power of 0.367 kW. For the handled electric vehicle, a battery pack consisting of 360 modules with approximately 135 kW was considered. The amount of waste heat obtained from this battery module is 0.0172 kW, and the amount of waste heat obtained from the total battery module is 6.192 kW. In this regard, considering the waste heat, the density of the heater is stated as 1.10 kW/m^2 (0.91 m^2/kW) for a battery module. The temperature variation for the non-cooled case is given in Fig. 8.

According to Fig. 8, the maximum temperatures (T_{max}) are evaluated for different DoD levels. For a fully charged battery (DoD = 0), the maximum temperatures at discharge rates of 1C, 2C, 3C, 4C, and 5C were determined as 303.51 K, 309.83 K, 316.88 K, 324.53 K, and 332.57 K, respectively. For (DoD = 0.2), the maximum temperatures at discharge rates of 1C, 2C, 3C, 4C, and 5C were determined as 303.46 K, 309 36 K, 315.88 K, 322.34 K, and 328 K. For (DoD = 0.4), the maximum temperatures at discharge rates of 1C, 2C, 3C, 4C, and 5C were determined as it is 303.37 K, 308.55 K, 314.05 K, 319.43 K and 324.67 K. For (DoD = 0.6), the maximum temperatures at discharge rates of 1C, 2C, 3C, 4C and 5C were determined as it is 303.10 F, 307.02 K, 310.95 K, 314.95 K, 314.69 K and 318.38 K. For (DoD = 0.8), the maximum temperatures at discharge rates of 1C, 2C, 3C, 4C and 5C were determined as 302.34 K, 304.36 K, 306.13 K, 307.61 K and 308.84 K. The variation of the applied discharge rate has a significant effect on the thermal behavior of the battery. As the discharge rate increases, it is observed that the maximum temperatures formed on the battery surface also increase. The highest temperature was recorded as 332.57 K at a discharge rate of 5C when the battery was fully charged. It is seen that the discharge time of the battery decreases as the discharge rate of the battery increases. At the same time, the maximum temperatures decrease with the increase of DoD. The decrease in temperatures due to the increase in the discharge levels is that the number of ions transferred between the positive and negative poles of the battery decreases during the discharge process. A decrease in the number of ions reduces the number of electrons transferred between the two poles. Fig. 9 shows the temperature variations at various locations of the Li-ion battery for discharge periods of 1C—5C at DoD = 0. As mentioned earlier, high temperatures on the battery surface can produce harmful effects on the

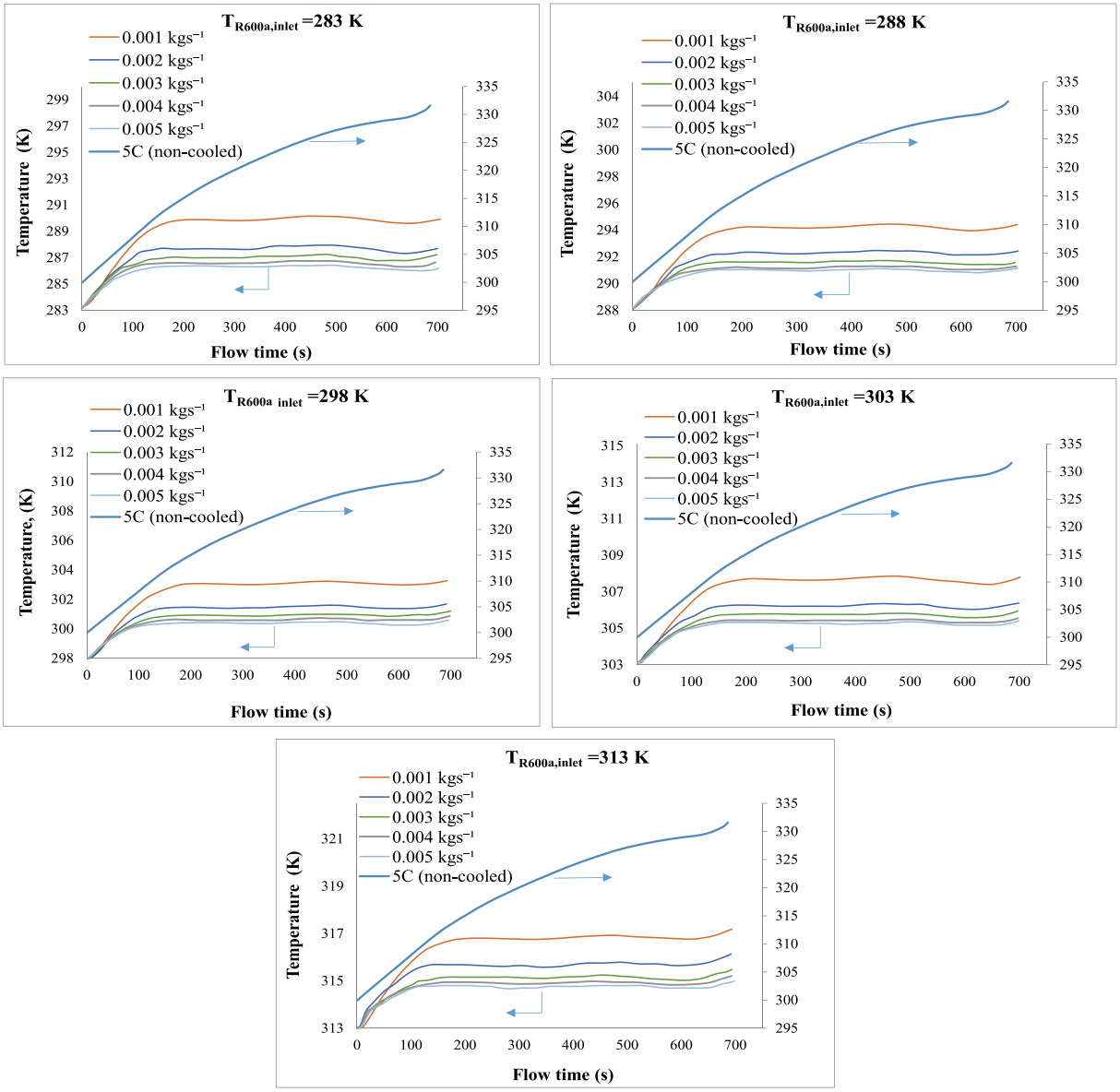

Fig. 12. Temperature variation for the different mass rates of R600a at 5C discharge rate.

Lithium-ion cell and cause the battery module to fail.

According to Fig. 9a, the maximum and minimum battery temperatures for the 1C discharge rate were observed, ranging between 303.2546 K and 303.4601 K. The maximum temperature difference was recorded as 0.2055 K, approximately a homogenous surface. According to Fig. 9b, the maximum and minimum temperatures at the 2C discharge rate were between 309.5776 K and 310.0703 K, with a temperature difference of 0.4927 K. According to Fig. 9c, the maximum and minimum temperatures at the 3C discharge rate were between 315.8276 K and 316.9628 K. The temperature difference is 1.1352 K. According to 9d, at a discharge rate of 4C, the maximum and minimum temperatures are 322.322 K and 324.218 K, with a temperature difference of 1.8957 K. According to Fig. 9e, the maximum and minimum temperatures at 5C discharge rate are between 331.5722 K and 328,487 K with a temperature difference of 3.0852 K. It is observed that the temperature distributions are more homogeneous at 1C discharge rate compared to other discharge rates. Because the longest flow time is obtained for a discharge rate of 1C, the heat conduction time at the battery surface is sufficient. It was observed that the temperatures formed on the battery surface increased due to the increase in the discharge rate. When Fig. 9b, c, d, and e are examined, it is seen that an almost homogeneous temperature distribution is realized in all of them. It is seen that the changes in the discharge parameters also change the thermal distributions. It is seen that the battery temperature is at the minimum value at the edge positions of the battery, while the maximum temperature is at the peak value in the upper middle parts of the battery. The obtained results are compatible with the literature [28]. In Fig. 9e, T_{max} was obtained with the highest temperature and C ratio. At the same time, the shortest flow time was obtained at the highest discharge rate of 5C. The increase in the C ratio causes temperature increases by accelerating the electrochemical reactions occurring in the cell, and the homogeneity of the temperature distributions on the battery surface decreases as the discharge times will be shortened in parallel with the applied discharge current.

For the cooled case, R600a as the cooling media was performed. In this case, the dual phase, including the gas and liquid phases, was evaluated since the phase change process results in higher heat transfer ratios depending on the higher heat transfer coefficients. Different inlet temperatures (283 K, 288 K, 298 K, 303 K, and 313 K) of R600a were investigated along with the different mass rates (0.001 kgs^{-1}, 0.002 kgs^{-1}, 0.003 kgs^{-1}, 0.004 kgs^{-1}, and 0.005 kgs^{-1}). The variation of the

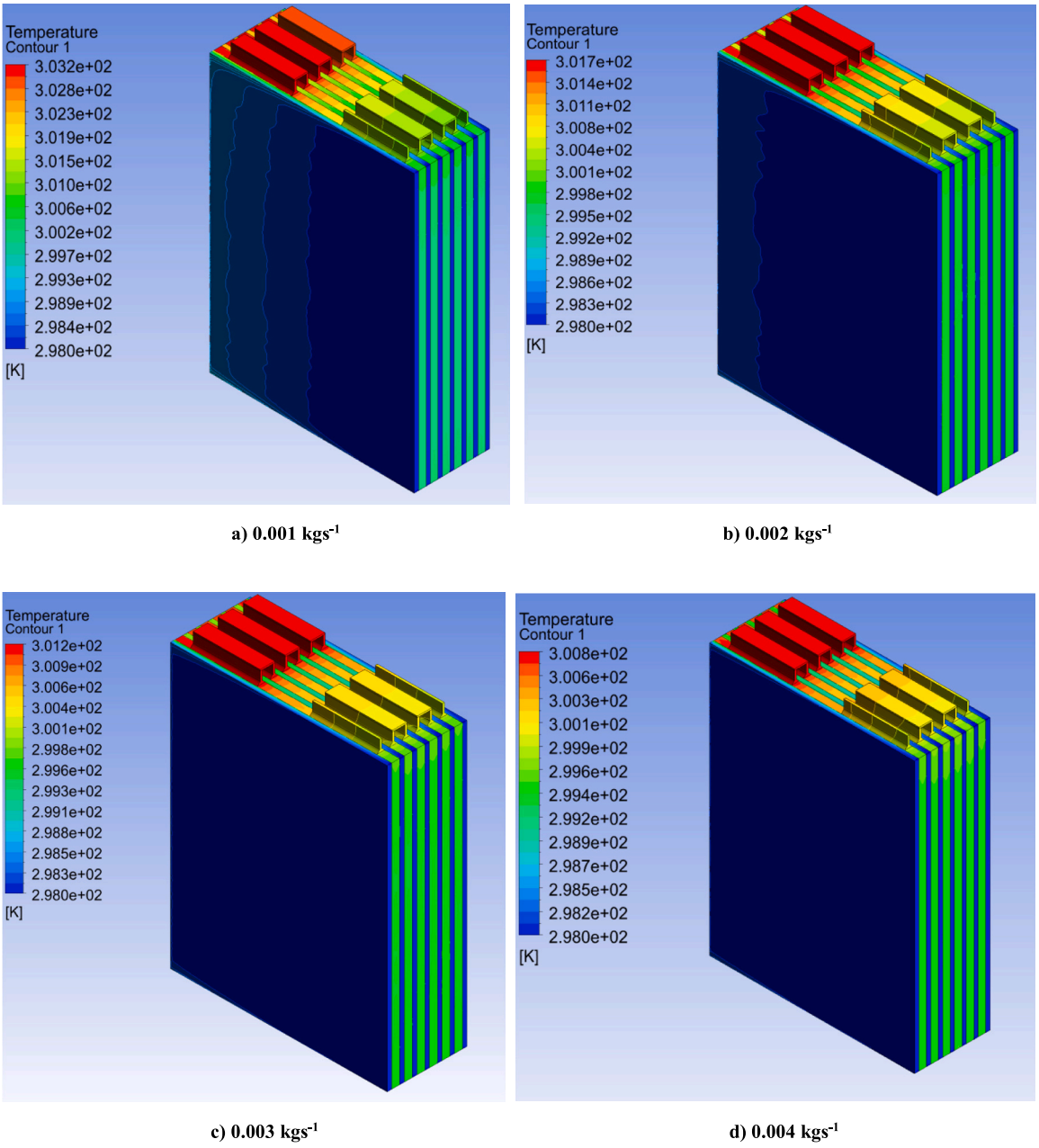

a) 0.001 kgs^{-1} **b) 0.002 kgs^{-1}**

c) 0.003 kgs^{-1} **d) 0.004 kgs^{-1}**

Fig. 13. The thermal distribution of the cooled battery unit.

heat transfer coefficients for 5C is given in Fig. 10.

According to Fig. 10, it can be seen that the change of heat transfer coefficients according to different fluid inlet temperatures has similar trends. When the fluid inlet temperature was 283 K, minimum and maximum heat transfer coefficients were recorded as 1.31–2.22, 2.05–3.28, 2.88–4.08, 3.44–4.80, 4.17–5.50 kWm^{-2} K^{-1} for the fluid mass rate of 0.001 kgs^{-1}, 0.002 kgs^{-1}, 0.003 kgs^{-1}, 0.004 kgs^{-1} and 0.005kgs^{-1}, respectively. For 288 K, these values were recorded as 1.17–2.12, 1.97–3.14, 2.65–3.91, 3.3–4.61, 4.05–5.27 kWm^{-2} K^{-1} for the fluid mass rate of 0.001 kgs^{-1}, 0.002 kgs^{-1}, 0.003 kgs^{-1}, 0.004 kgs^{-1} and 0.005kgs^{-1}, respectively. For 298 K, these values were recorded as 1.18–1.93, 1.76–2.88, 2.48–3.58, 3.02–4.23, 3.72–4.85 kWm^{-2} K^{-1} for the fluid mass rate of 0.001 kgs^{-1}, 0.002 kgs^{-1}, 0.003 kgs^{-1}, 0.004 kgs^{-1} and 0.005kgs^{-1}, respectively. For 303 K, these values were recorded as 1.15–1.83, 1.76–2.68, 2.30–3.36, 3.05–3.98, 3.54–4.56 kWm^{-2} K^{-1} for the fluid mass rate of 0.001 kgs^{-1}, 0.002 kgs^{-1}, 0.003 kgs^{-1}, 0.004 kgs^{-1} and 0.005kgs^{-1}, respectively. For 313 K, these values were recorded as 1.10–1.68, 1.62–2.52, 2.14–3.20, 2.53–3.72, 3.14–4.27 kWm^{-2} K^{-1} for the fluid mass rate of 0.001 kgs^{-1}, 0.002 kgs^{-1}, 0.003 kgs^{-1}, 0.004 kgs^{-1} and 0.005kgs^{-1}, respectively. The change in the fluid inlet temperatures also changes the heat transfer coefficient. The highest heat transfer coefficients were recorded as 5.496 kWm^{-2} K^{-1} for the flow rate of 0.005 kgs^{-1} and a fluid inlet temperature of 283 K. The lowest heat transfer coefficients were obtained as 1.10 kWm^{-2} K^{-1} for a fluid flow rate of 0.001 kgs^{-1} and a fluid inlet temperature of 313 K. In Fig. 11, the temperature distributions are given for the different fluid inlet temperatures and discharge rates with the mass flow rate of 0.005 kgs^{-1}.

According to Fig. 11, it is seen that the change of the C ratio is effective on the temperature distribution. When the C ratio increases, more current is supplied to the battery. The higher the discharge current applied to the battery during the discharge process, the higher the maximum temperature difference at the battery surface occurs. For this

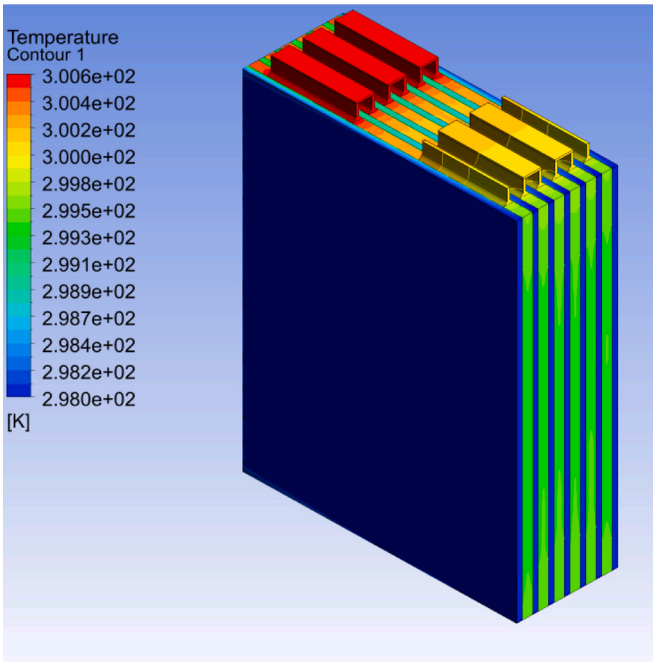

e) 0.005 kgs^{-1}

Fig. 13. (*continued*).

reason, the generated heat in the battery increases. It can be more difficult to effectively dissipate this heat by conductive materials and conventional air-cooled systems. As a result, the temperature rise and the temperature difference at the battery become more noticeable. When the refrigerant inlet temperature was regulated to 25 °C, the maximum temperature differences were recorded as 0.415 K, 0.731 K, 1.445 K, 1.731 K, and 2.597 K for discharge rates 1C, 2C, 3C, 4C, and 5C, respectively. Similar results were recorded for the other cases. The lower refrigerant inlet temperatures allow more effective cooling of the battery. As the refrigerant inlet temperature increases, battery cooling efficiency decreases. The change in fluid inlet temperature can affect battery cooling performance and determine battery operating temperature. However, to achieve the best performance from lithium-ion batteries, the batteries must operate within certain operating temperature ranges. Therefore, the fluid inlet temperature must be controlled within a specific range. This ensures that the battery is maintained within the desired operating temperature range. CFD analyses were also conducted for the cooled case of the battery by running the observed heat transfer coefficients at different mass rates of R600a. The temperature variation of the Li-ion battery unit at 5C is shown in Fig. 12.

According to Fig. 12, the maximum temperature of the battery was recorded as 331.57 K for the non-cooled case. When the fluid inlet temperature is 283 K, and the fluid inlet velocities are selected, the maximum temperatures and their corresponding maximum temperature differences were obtained as 289.6744 K and 3.6744 K, 287.5390 K and 2.5390 K, 286.8509 K and 2.4547 K, 286.4448 K and 2.1835 K, 286.1870 K, and 1.9584 K for the R600a inlet mass rates of 0.001 kgs^{-1}, 0.002 kgs^{-1}, 0.003 kgs^{-1}, 0.004 kgs^{-1}, and 0.005 kgs^{-1}, respectively. For a refrigerant inlet temperature of 288 K, these values were recorded as 293.9554 K and 4.0144 K, 292.1768 K and 3.3256 K, 291.4772 K and 2.8995 K, 291.1526 K and 2.5875 K, 290.929 K and 2.0842 K. For 298 K, these values were recorded as 303.1883 K and 4.2174 K, 301.6749 K and 3.6054 K, 301.1578 K and 2.8215 K, 300.8001 K, and 2.3513 K 300.6254 K and 2.1226 K. For 303 K, these values were recorded as 307.7168 K and 4.5326 K, 306.4776 K and 3.6048 K, 305.8454 K and 3.2076 K, 305.5620 K and 2.862 K, and 305.3954 K and 2.6657 K. For 313 K, these values were recorded as 317.3145 K and 4.539 K, 315.9219 K and 3.8457 K, 315.5819 K and 3.0743 K, 315.3333 K and 2.8584 K, 315.2057 and 2.7044 K. The temperature distribution of the Li-ion battery for discharge periods of 1C—5C and DoD = 0 is given in Fig. 13.

According to Fig. 13, when the temperature distribution of the battery module is examined according to the fluid inlet velocity, it is seen that the temperature of the battery decreases as the liquid inlet velocity increases. At the same time, the maximum temperature difference also decreases. The temperature at the positive tabs is higher than at the negative tabs due to the lower electrical conductivity of the positive electrode. When the battery module is generally examined, the temperature is 303.1883 K at a liquid inlet speed of 0.001 kgs^{-1} and 300.6254 K at a liquid inlet rate of 0.005 kgs^{-1}. The temperature difference on the battery surface decreased from 4.4174 K to 2.1226 K. The temperature distributions on the battery surface become more homogeneous with the increase in the fluid inlet velocity. Cooling has been observed to be more effective at higher fluid velocities by reducing the maximum temperature differences on the coil surface. In addition, since the inlet and outlet temperatures of the refrigerant are approximately the same due to phase change, the temperature distributions on the battery surface are more uniform.

When the numerically obtained data were evaluated, the battery temperature was kept within the appropriate working temperature ranges, with temperature variances of <5 °C as appropriate to the literature [22,57]. Due to the higher heat transfer coefficients of the chosen refrigerant, cooling efficiency could effectively be achieved. The optimal operating temperatures for the battery were determined as 288 K, 298 K, and 303 K. This extends the life and performance of the Li-ion battery cell. The temperature changes of the batteries are acceptable at all refrigerant inlet temperatures. The battery unit was kept within the desired temperature range for each fluid inlet rate. However, in cases where the fluid inlet temperature is below 288 K and above 313 K, the battery module is not kept within the desired temperature ranges. These operating temperatures can compromise the long-term operating performance of the battery module. The other important parameter of dual-phase cooling is the vapor quality (x) since R600a was aimed to be used in an auxiliary system. The variation of the vapor quality for 5C is given in Fig. 14.

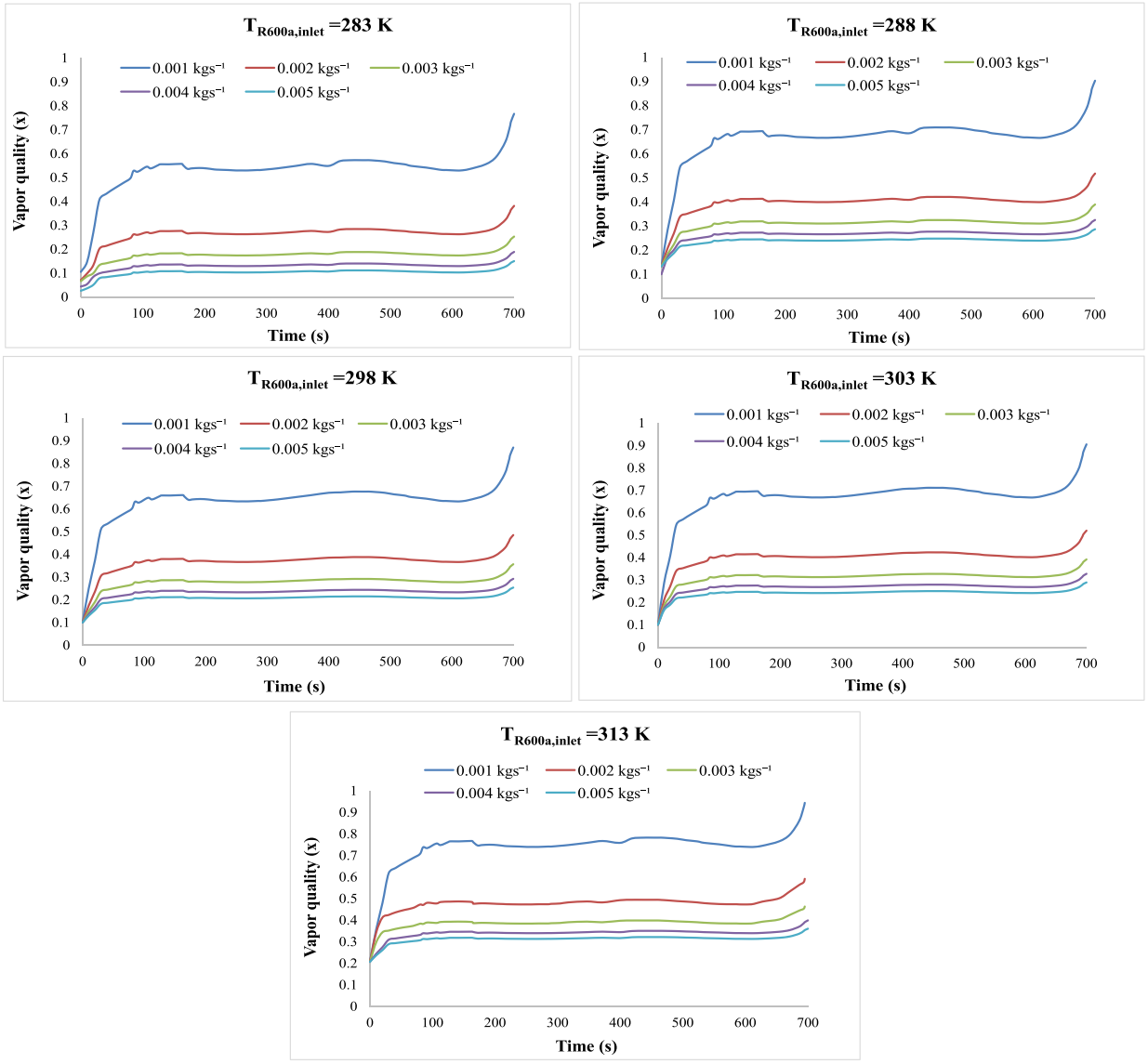

Fig. 14. Variation of the vapor quality (x) for different inlet temperatures at 5C.

According to Fig. 14, the highest vapor quality was obtained as 0.97 at a mass flow rate of 0.001 kgs^{-1} and the refrigerant inlet temperature of 313 K. The lowest vapor quality (or degree of dryness) was obtained as 0.15 at a mass flow rate of 0.005 kgs^{-1} and a refrigerant inlet temperature of 283 K. When the fluid inlet temperature was 283 K, the maximum dryness degree was recorded as 0.76 for the R600a inlet mass ratio of 0.001 kgs^{-1}. For the fluid inlet temperature of 288 K at the R600a inlet mass ratio of 0.001 kgs^{-1}, the maximum dryness degree was recorded as 0.90. For 298 K at the R600a inlet mass ratio of 0.001 kgs^{-1}, the maximum dryness degree was recorded as 0.87. For 303 K at the R600a inlet mass ratio of 0.001 kgs^{-1}, the maximum dryness degree was recorded as 0.90.

Considering an approximately 135 kW power output, an electric vehicle needs 360 battery modules. When the inlet fluid temperature is 283 K, the maximum amount of R600a to be used in the secondary cycle was recorded as 0.2820 kgs^{-1}. For the inlet fluid temperature of 288 K, it was recorded as 0.5169 kgs^{-1}. For the inlet fluid temperature of 298 K, these amounts were recorded as 0.4576 kgs^{-1}. For 303 K, it was recorded as 0.5208 kgs^{-1}. For the inlet fluid temperature of 313 K, it was recorded as 0.6559 kgs^{-1}.

4. Conclusions

In this study, a thermal management system of Li-ion batteries for an electric vehicle was analyzed. In this regard, a battery system including 360 modules for a 135 kW electric vehicle was proposed. In the study, it was aimed to evaluate the waste heat of the battery modules in the auxiliary systems such as thermoelectric units and air-conditioning systems. Therefore, a two-phase heat transfer phenomena was conducted through the computational fluid dynamics (CFD) analysis using ANSYS software since the boiling heat transfer mechanism has a higher heat transfer coefficient. R600a was chosen as the cooling media in the thermal management process considering the auxiliary use. The considerable heat transfer coefficients ranging between 1.10 and 5.49 $kWm^{-2}\ K^{-1}$ were determined, which are higher than the conventional air-cooled system. The cooled module temperature was recorded between 290.93 K and 317.31 K, whereas it was recorded as 332.57 K for the non-cooled system. For secondary purposes, the refrigerant mass rate ranging between 0.2760 kgs^{-1} and 0.6559 kgs^{-1} was obtained. The temperature of the refrigerant was determined in the range of 283 K and 313 K. So, the handled two-phase thermal management of the battery system was found useful for secondary use such as thermoelectric unit and heat pump system (heating mode) of the electric vehicles.

The most significant disadvantage of using refrigerant is the risk of flame. However, the working conditions of the battery modules are within reasonable limits. Also, the available refrigerants should be considered at this point. The secondary cycles should also be carefully designed and optimized under the obtained results.

Nomenclature

Cp	specific heat ($Jkg^{-1}K^{-1}$)
F	forced convection-boiling factor
G	mass velocity
h	heat transfer coefficient ($kWm^{-2}K^{-1}$)
J	current density
j_{ECh}	volumetrically current transfer ratio
$_{Short}$	current transfer ratio
k	heat conductivity ($Wm^{-1}K^{-1}$)
$\dot{m}$	mass flow rate (kgs^{-1})
P	pressure
S	effectiveness factor
Pr	Prandtl number
Re	Reynolds number
t	time (s)
T	temperature (K)
T_{inlet}	fluid inlet temperature (K)
$\Delta T_{\max}$	maximum battery temperature difference
v	velocity (ms^{-1})
V	operational voltage (V)
Q_g	heat generation
q^*	heat flow
U	NTGK variable
Y	NTGK variable

Subscripts

f	saturated liquid
g	saturated vapor
max	maximum
k	bubble boiling
z	forced convection coefficients

Greek symbols

∇	gradient operator
a	degree of conversion
ρ	density (kgm^{-3})
μ	viscosity ($kgm^{-1}s^{-1}$)
σ	surface tension
σ_+	effective electric conductivities for the positive electrodes
σ_-	effective electric conductivities for the negative electrodes
φ_+	phase potentials for the positive electrodes
φ_-	phase potentials for the negative electrodes

Acronyms

3D	three-dimensional
CFD	computational fluid dynamics
C-rate	current discharge rate
DoD	depth of discharge
EV	electric vehicles
BTMS	battery thermal management system
ORC	organic Rankine cycle
NTGK	Newman-Tiedemann-Gu-Kim
PCM	phase change materials
SoC	state of charge

CRediT authorship contribution statement

Ahmet Mavi: Analysis, Data curation, Methodology, Investigation, Writing.

Oguz Arslan: Analysis, Conceptualization, Methodology, Validation, Writing - Reviewing and Editing, Investigation.

Declaration of competing interest

The authors declare that they have no known competing financial interests or personal relationships that could have appeared to influence the work reported in this paper.

Data availability

No data was used for the research described in the article.

References

[1] J.I.A. Shunping, P. Hongqin, L.I.U. Shuang, Z. Xiaojie, Review of transportation and energy consumption related research, J. Transp. Syst. Eng. Inf. Technol. 9 (3) (2009) 6–16, https://doi.org/10.1016/S1570-6672(08)60061-6.

[2] S. Amjad, S. Neelakrishnan, R. Rudramoorthy, Review of design considerations and technological challenges for successful development and deployment of plug-in hybrid electric vehicles, Renew. Sustain. Energy Rev. 14 (2010) 1104–1110, https://doi.org/10.1016/j.rser.2009.11.001.

[3] W. Masayoshi, Research and development of electric vehicles for clean transportation, J. Environ. Sci. 21 (6) (2009) 745–749, https://doi.org/10.1016/S1001-0742(08)62335-9.

[4] M. Farag, H. Sweity, M. Fleckenstein, S. Habibi, Combined electrochemical, heat generation, and thermal model for large prismatic lithium-ion batteries in real-time applications, J. Power Sources 360 (2017) 618–633, https://doi.org/10.1016/j.jpowsour.2017.06.031.

[5] M. Ghalkhani, F. Bahiraei, G. Nazri, M. Saif, Electrochemical – thermal model of pouch-type lithium-ion batteries, Electrochim. Acta 247 (2017) 569–587, https://doi.org/10.1016/j.electacta.2017.06.164.

[6] F. Karipoğlu, M.S. Genç, B. Akarsu, GIS-based optimal site selection for the solar-powered hydrogen fuel charge stations, Fuel 324 (2022), 124626, https://doi.org/10.1016/j.fuel.2022.124626.

[7] B. Akarsu, M.S. Genç, Optimization of electricity and hydrogen production with hybrid renewable energy systems, Fuel 324 (PA) (2022), 124465, https://doi.org/10.1016/j.fuel.2022.124465.

[8] X. Zhang, Z. Li, L. Luo, Y. Fan, Z. Du, A review on thermal management of lithium-ion batteries for electric vehicles, Energy 238 (2022), 121652, https://doi.org/10.1016/j.energy.2021.121652.

[9] C. Zhao, W. Cao, T. Dong, F. Jiang, Thermal behavior study of discharging/charging cylindrical lithium-ion battery module cooled by channeled liquid flow, Int. J. Heat Mass Transf. 120 (2018) 751–762, https://doi.org/10.1016/j.ijheatmasstransfer.2017.12. 083.

[10] J. Chen, S. Kang, E. Jiaqiang, Z. Huang, K. Wei, B. Zhang, H. Zhu, Y. Deng, F. Zhang, G. Liao, J., Effects of different phase change material thermal management strategies on the cooling performance of the power lithium ion batteries: a review, J. Power Sources 442 (October) (2019), 227228, https://doi.org/10.1016/j.jpowsour.2019.227228.

[11] J. Xun, R. Liu, K. Jiao, Numerical and analytical modeling of lithium ion battery thermal behaviors with different cooling designs, J. Power Sources 233 (2013) 47–61, https://doi.org/10.1016/j.jpowsour. 2013.01.095.

[12] Q. Wang, B. Jiang, B. Li, Y. Yan, A critical review of thermal management models and solutions of lithium-ion batteries for the development of pure electric vehicles, Renew. Sustain. Energy Rev. 64 (2016) 106–128, https://doi.org/10.1016/j.rser.2016.05.033.

[13] Q. Wang, P. Ping, X. Zhao, G. Chu, J. Sun, C. Chen, Thermal runaway caused fire and explosion of lithium ion battery, J. Power Sources 208 (2012) 210–224, https://doi.org/10.1016/j.jpowsour.2012.02. 038.

[14] H. Mbulu, Y. Laoonual, S. Wongwises, Experimental study on the thermal performance of a battery thermal management system using heat pipes, Case Stud. Therm. Eng. 26 (2021), 101029, https://doi.org/10.1016/j.csite.2021.101029.

[15] Y. Deng, C. Feng, E. Jiaqiang, H. Zhu, J. Chen, Effects of different coolants and cooling strategies on the cooling performance of the power lithium ion battery system: a review, Appl. Therm. Eng. 142 (June) (2018) 10–29, https://doi.org/10.1016/j.applthermaleng.2018.06.043.

[16] S. Panchal, R. Khasow, I. Dincer, M. Agelin-chaab, R. Fraser, M. Fowler, Thermal design and simulation of mini-channel cold plate for water cooled large sized prismatic lithium-ion battery, Appl. Therm. Eng. 122 (2017) 80–90, https://doi.org/10.1016/j.applthermaleng.2017.05.010.

[17] O. Kalkan, A. Celen, K. Bakirci, Experimental and numerical investigation of the LiFePO 4 battery cooling by natural convection, J. Energy Storage 40 (May) (2021), 102796, https://doi.org/10.1016/j.est.2021.102796.

[18] C. Huberand, R. Kuhn, Thermal management of batteries for electric vehicles, in: B. Scrosati, J. Garche, W. Tillmetz (Eds.), Advances in Battery Technologies for

Electric Vehicles, Woodhead Publishing, 2015, pp. 327–358, https://doi.org/10.1016/B978-1-78242-377-5.00013-3.
[19] U. Moralı, Computational modeling and statistical evaluation of thermal behavior of cylindrical lithium-ion battery, Journal of Energy Storage 55 (May) (2022), 105376, https://doi.org/10.1016/j.est.2022.105376.
[20] V. Lucaferri, et al., Modeling and optimization method for Battery Energy Storage Systems operating at variable C-rate: a comparative study of Lithium technologies, J. Energy Storage 73 (PD) (2023), 109232, https://doi.org/10.1016/j.est.2023.109232.
[21] S. Gocmen, S. Gungor, E. Cetkin, Thermal management of electric vehicle battery cells with homogeneous coolant and temperature distribution, J. Appl. Phys. 127 (23) (2020), 234902, https://doi.org/10.1063/5.0004453.
[22] O. Yetik, T. Hikmet, A numerical study on the thermal performance of prismatic li-ion batteries for hibrid electric aircraft, Energy 195 (2020), 117009, https://doi.org/10.1016/j.energy.2020.117009.
[23] R. Zhao, J. Gu, J. Liu, An investigation on the signi fi cance of reversible heat to the thermal behavior of lithium ion battery through simulations, J. Power Sources 266 (2014) 422–432, https://doi.org/10.1016/j.jpowsour.2014.05.034.
[24] R. Mahamud, C. Park, Reciprocating air flow for Li-ion battery thermal management to improve temperature uniformity, J. Power Sources 196 (13) (2011) 5685–5696, https://doi.org/10.1016/j.jpowsour.2011.02.076.
[25] H. Xu, X. Zhang, G. Xiang, H. Li, Optimization of liquid cooling and heat dissipation system of lithium-ion battery packs of automobile, Case Stud. Therm. Eng. 26 (2021), 101012, https://doi.org/10.1016/j.csite.2021.101012.
[26] A. Babapoor, M. Azizi, G. Karimi, Thermal management of a Li-ion battery using carbon fiber-PCM composites, Appl. Therm. Eng. 82 (2015) 281–290, https://doi.org/10.1016/j.applthermaleng.2015.02.068.
[27] L.W. Jin, P.S. Lee, X.X. Kong, Y. Fan, S.K. Chou, Ultra-thin minichannel LCP for EV battery thermal management, Appl. Energy 113 (2014) 1786–1794, https://doi.org/10.1016/j.apenergy.2013.07.013.
[28] P. Ping, R. Peng, D. Kong, G. Chen, J. Wen, Investigation on thermal management performance of PCM-fin structure for Li-ion battery module in high-temperature environment, Energ. Conver. Manage. 176 (September) (2018) 131–146, https://doi.org/10.1016/j.enconman.2018.09.025.
[29] R. Zhao, J. Gu, J. Liu, An experimental study of heat pipe thermal management system with wet cooling method for lithium ion batteries, J. Power Sources 273 (2015) 1089–1097, https://doi.org/10.1016/j.jpowsour.2014.10.007.
[30] J. Wang, S. Lu, Y. Wang, C. Li, K. Wang, Effect analysis on thermal behavior enhancement of lithium – ion battery pack with different cooling structures, J. Energy Storage 32 (September) (2020), 101800, https://doi.org/10.1016/j.est.2020.101800.
[31] X. Yu, Z. Lu, L. Zhang, L. Wei, X. Cui, L. Jin, Experimental study on transient thermal characteristics of stagger-arranged lithium-ion battery pack with air cooling strategy, Int. J. Heat Mass Transf. 143 (2019), 118576, https://doi.org/10.1016/j.ijheatmass-transfer.2019.118576.
[32] S. Xin, C. Wang, H. Xi, Thermal management scheme and optimization of cylindrical lithium-ion battery pack based on air cooling and liquid cooling, Appl. Therm. Eng. 224 (September 2022) (2023), 120100, https://doi.org/10.1016/j.applthermaleng.2023.120100.
[33] Z. Rao, Q. Wang, C. Huang, Investigation of the thermal performance of phase change material/mini-channel coupled battery thermal management system, Appl. Energy 164 (2016) 659–669, https://doi.org/10.1016/j.apenergy.2015.12.021.
[34] Z. Guo, Y. Wang, S. Zhao, T. Zhao, M. Ni, Modeling and optimization of micro heat pipe cooling battery thermal management system via deep learning and multi-objective genetic algorithms, Int. J. Heat Mass Transf. 207 (2023), 124024, https://doi.org/10.1016/j.ijheatmasstransfer.2023.124024.
[35] D. Dan, C. Yao, Y. Zhang, H. Zhang, Z. Zeng, X. Xu, Dynamic thermal behavior of micro heat pipe array-air cooling battery thermal management system based on thermal network model, Appl. Therm. Eng. 162 (July) (2019), 114183, https://doi.org/10.1016/j.applthermaleng.2019.114183.
[36] J. Kim, J. Oh, H. Lee, Review on battery thermal management system for electric vehicles, Appl. Therm. Eng. 149 (September 2018) (2019) 192–212, https://doi.org/10.1016/j.applthermaleng.2018.12.020.
[37] S. Shahid, M. Agelin-chaab, Development and analysis of hybrid cooling concepts for an electric battery pack, J. Energy Storage 73 (PA) (2023), 108952, https://doi.org/10.1016/j.est.2023.108952.
[38] S. Chavan, J. Liu, B. Venkateswarlu, S.W. Joo, S.C. Kim, Numerical simulation of lithium-ion battery thermal management systems: a comparison of fluid flow channels and cooling fluids, J. Energy Storage 73 (PB) (2023), 108940, https://doi.org/10.1016/j.est.2023.108940.
[39] K.P. Drummond, et al., A hierarchical manifold microchannel heat sink array for high-heat-flux two-phase cooling of electronics, Int. J. Heat Mass Transf. 117 (2018) 319–330, https://doi.org/10.1016/j.ijheatmasstransfer.2017.10.015.
[40] E.J. Choi, J.Y. Park, M.S. Kim, Two-phase cooling using HFE-7100 for polymer electrolyte membrane fuel cell application, Appl. Therm. Eng. 148 (August 2018) (2019) 868–877, https://doi.org/10.1016/j.applthermaleng.2018.11.103.
[41] E.J. Choi, J.Y. Park, M.S. Kim, ScienceDirect a comparison of temperature distribution in PEMFC with single-phase water cooling and two-phase HFE-7100 cooling methods by numerical study, Int. J. Hydrogen Energy 43 (29) (2018) 13406–13419, https://doi.org/10.1016/j.ijhydene.2018.05.056.
[42] T. Zhang, J.T. Wen, Y. Peles, J. Catano, R. Zhou, M.K. Jensen, Two-phase refrigerant flow instability analysis and active control in transient electronics cooling systems, Int. J. Multiph. Flow 37 (1) (2011) 84–97, https://doi.org/10.1016/j.ijmultiphaseflow.2010. 07.003.
[43] P. Zhang, X. Wei, L. Yan, H. Xu, T. Yang, Review of recent developments on pump-assisted two-phase flow cooling technology, Appl. Therm. Eng. 150 (January) (2019) 811–823, https://doi.org/10.1016/j.applthermaleng.2018.12.169.
[44] L. Jie, L. Mou, G. Kai-hua, H. Zhen-hui, L. Ting-xuen, Experimental investigation on start-up of mechanically pumped cooling loop, Energy Conv. Manag. 49 (10) (Oct. 2008) 2595–2601, https://doi.org/10.1016/j.enconman.2008.05.007.
[45] Q. Gao, Y. Liu, G. Wang, F. Deng, J. Zhu, An experimental investigation of refrigerant emergency spray on cooling and oxygen suppression for overheating power battery, J. Power Sources 415 (September 2018) (2019) 33–43, https://doi.org/10.1016/j.jpowsour.2019.01.052.
[46] M. Al-zareer, I. Dincer, M.A. Rosen, Heat and mass transfer modeling and assessment of a new battery cooling system, Int. J. Heat Mass Transf. 126 (2018) 765–778, https://doi.org/10.1016/j.ijheatmasstransfer.2018.04.157.
[47] M. Al-zareer, I. Dincer, M.A. Rosen, A thermal performance management system for lithium-ion battery packs, Appl. Therm. Eng. 165 (August 2019) (2020), 114378, https://doi.org/10.1016/j.applther-maleng.2019.114378.
[48] S. Park, D.S. Jang, D. Lee, S.H. Hong, Y. Kim, Simulation on cooling performance characteristics of a refrigerant-cooled active thermal management system for lithium ion batteries, Int. J. Heat Mass Transf. 135 (2019) 131–141, https://doi.org/10.1016/j.ijheatmasstransfer.2019.01.109.
[49] H.S. Hamut, I. Dincer, G.F. Naterer, Performance assessment of thermal management systems for electric and hybrid electric vehicles, Int. J. Energy Res. 37 (2013) 1–12, https://doi.org/10.1002/er.1951.
[50] Y. Wang, et al., Experimental studies on two-phase immersion liquid cooling for Li-ion battery thermal management, J. Energy Storage 72 (PE) (2023), 108748, https://doi.org/10.1016/j.est.2023.108748.
[51] C. Liu, H. Yu, Evaluation and optimization of a two-phase liquid-immersion cooling system for data centers, Energies 14 (5) (2021) 1395, https://doi.org/10.3390/en14051395.
[52] M. Goodarzi, H. Jannesari, M. Ameri, Experimental study of Li-ion battery thermal management based on the liquid-vapor phase change in direct contact with the cells, J. Energy Storage 62 (June 2022) (2023), 106834, https://doi.org/10.1016/j.est.2023.106834.
[53] N.P. Williams, D. Trimble, S.M.O. Shaughnessy, Liquid immersion thermal management of lithium-ion batteries for electric vehicles: an experimental study, J. Energy Storage 72 (PD) (2023), 108636, https://doi.org/10.1016/j.est.2023.108636.
[54] H. Chen, T. Zhang, Q. Gao, Z. Han, Y. Xu, Advance and prospect of power battery thermal management based on phase change and boiling heat transfer, J. Energy Storage 53 (June) (2022), 105254, https://doi.org/10.1016/j.est.2022.105254.
[55] I. Karasu, M.S. Genc, H.H. Acikel, Numerical study on low Reynolds number flows over an aerofoil, J. Appl. Mech. Eng. 2 (2013), 1000131.
[56] H. Zhang, C. Li, R. Zhang, Y. Lin, H. Fang, Thermal analysis of a 6s4p Lithium-ion battery pack cooled by cold plates based on a multi-domain modeling framework, Appl. Therm. Eng. 173 (December 2019) (2020), 115216, https://doi.org/10.1016/j.applthermaleng.2020.115216.
[57] J. Newman, W. Tiedemann, Potential and current distribution in electrochemical cells: interpretation of the half-cell voltage measurements as a function of reference-electrode location, J. Electrochem. Soc. 140 (7) (1993) 1961–1968.
[58] J. Kim, C. Yang, J. Lamb, A. Kurzawski, J. Hewson, L. Torres-Castro, A. Mallarapu, S. Santhanagopalan, A comprehensive numerical and experimental study for the passive thermal management in battery modules and packs, J. Electrochem. Soc. 169 (11) (2022), 110543, https://doi.org/10.1149/1945-7111/ac9ee4.
[59] U.S. Kim, C.B. Shin, C.S. Kim, Modeling for the scale-up of a lithium-ion polymer battery, J. Power Sources 158 (1) (2009) 841–846, https://doi.org/10.1016/j.jpowsour.2008.10.019.
[60] S. Chacko, Y.M. Chung, Thermal modelling of Li-ion polymer battery for electric vehicle drive cycles, J. Power Sources 213 (2012) 296–303, https://doi.org/10.1016/j.jpowsour.2012.04.015.
[61] S. Allu, S. Kalnaus, W. Elwasif, S. Simunovic, J.A. Turner, A new open computational framework for highly-resolved coupled three-dimensional multiphysics simulations of Li-ion cells, J. Power Sources 246 (2014) 876–886, https://doi.org/10.1016/j.jpowsour.2013.08.040.
[62] H. Gu, Mathematical analysis of a Zn/NiOOH cell, J. Electrochem. Soc. 130 (7) (1983) 1459.
[63] U.S. Kim, J. Yi, C.B. Shin, T. Han, S. Park, Modeling the dependence of the discharge behavior of a lithium-ion battery on the environmental temperature, J. Electrochem. Soc. 158 (5) (2011) 1–8, https://doi.org/10.1149/1.3565179.
[64] S. Liu, T. Zhang, C. Zhang, L. Yuan, Z. Xu, L. Jin, Non-uniform heat generation model of pouch lithium-ion battery based on regional heat generation rate, J. Energy Storage 63 (February) (2023), 107074, https://doi.org/10.1016/j.est.2023.107074.
[65] Q. Wang, Q. Sun, P. Ping, X. Zhao, J. Sun, Z. Lin, Heat transfer in the dynamic cycling of lithium – titanate batteries, Int. J. Heat Mass Transf. 93 (2016) 896–905, https://doi.org/10.1016/j.ijheatmasstransfer.2015.11.007.
[66] Q. Huang, M. Yan, Z. Jiang, Thermal study on single electrodes in lithium-ion battery, J. Power Sources 156 (2) (2006) 541–546.
[67] K. Onda, T. Ohshima, M. Nakayama, K. Fukuda, T. Araki, Thermal behavior of small lithium-ion battery during rapid charge and discharge cycles, J. Power Sources 158 (2006) 535–542, https://doi.org/10.1016/j.jpowsour.2005.08.049.
[68] C. Forgez, D.V. Do, G. Friedrich, M. Morcrette, C. Delacourt, Thermal modeling of a cylindrical LiFePO4/graphite lithium-ion battery, J. Power Sources 195 (2010) 2961–2968, https://doi.org/10.1016/j.jpowsour.2009.10.105.
[69] T.M. Bandhauer, S. Garimella, T.F. Fuller, Temperature-dependent electrochemical heat generation in a commercial lithium-ion battery, J. Power Sources 247 (2014) 618–628, https://doi.org/10.1016/j. jpowsour.2013.08.015.

[70] D. Bernardi, E. Pawlikowski, J. Newman, A general energy balance for battery systems, J. Electrochem. Soc. 132 (1985) 5–12, https://doi.org/10.1149/1.2113792.
[71] M. Ouyang, Z. Chu, L. Lu, J. Li, X. Han, X. Feng, G. Liu, Low temperature aging mechanism identi fi cation and lithium deposition in a large format lithium iron phosphate battery for different charge profiles, J. Power Sources 286 (2015) 309–320, https://doi.org/10.1016/j.jpowsour.2015.03.178.
[72] K. Somasundaram, E. Birgersson, A. Sadashiv, Thermal – electrochemical model for passive thermal management of a spiral-wound lithium-ion battery, J. Power Sources 203 (2012) 84–96, https://doi.org/10.1016/j.jpowsour.2011.11.075.
[73] O. Arslan, M.A. Ozgur, R. Kose, Electricity generation ability of the Simav geothermal field: a technoeconomic approach, Energy Sources, Part A 34 (12) (2012) 1130–1144, https://doi.org/10.1080/15567031003773254.
[74] O. Arslan, D. Kilic, Concurrent optimization and 4E analysis of organic Rankine cycle power plant driven by parabolic trough collector for low-solar radiation zone, Sustain. Energy Technol. Assessments 46 (March) (2021), 101230, https://doi.org/10.1016/j.seta.2021.101230.
[75] A. Tugcu, O. Arslan, R. Kose, N. Yamankaradeniz, Thermodynamics and economical analysis of geothermal assisted absorption refrigeration system: Simav case study, J Turkish Soc Thermal Sci Technol. 36 (2016) 143–159.
[76] H. Yuncu, S. Kakac, Basic Heat Transfer, Bilim Publishing, Ankara, 1999 (in Turkish).
[77] H. Lv, H. Ma, N. Mao, T. He, Boiling heat transfer mechanism of environmental-friendly refrigerants: a review, Int. J. Refrig. 133 (August 2021) (2022) 214–225, https://doi.org/10.1016/j.ijrefrig.2021.10.007.